ISSN 1349-1113
JAXA-RR-06-020E

JAXA Research and Development Report

# Measurements of Turbulent Scalar Fluxes for Methane-Air Mixtures at Different Inlet Temperatures

Laurent ZIMMER , Shigeru TACHIBANA

March 2007

Japan Aerospace Exploration Agency

JAXA-RR-06-020E

JAXA Research and Development Report
宇宙航空研究開発機構研究開発報告

# Measurements of Turbulent Scalar Fluxes for Methane-Air Mixtures at Different Inlet Temperatures

入口温度の異なるメタンー空気予混合燃焼流の乱流スカラー流束計測

Laurent ZIMMER , Shigeru TACHIBANA
ジマー・ロレント、立花　繁

Aeroengine Technology Center, Institute of Aerospace Technology
総合技術研究本部　航空エンジン技術開発センター

March 2007
2007 年 3 月

Japan Aerospace Exploration Agency
宇宙航空研究開発機構

# Measurements of turbulent scalar fluxes for methane-air mixtures at different inlet temperatures*

Laurent ZIMMER*1, Shigeru TACHIBANA*1

**Abstract**

Simultaneous Particle Image Velocimetry / OH Planar Laser Induced Fluorescence (PIV / OH-PLIF) was used to measure the conditional unburned and burned velocities in turbulent premixed methane-air flames. The flames used were stabilized through a balance between the burning velocity and incoming flow, hence without a recirculation zone or stagnation plate. The turbulent intensity as well as the temperature at the inlet could be changed, so that turbulent scalar fluxes $\widetilde{\mu''c''}$ were measured at a velocity ratio ($u'/S_L$) ranging from 1 to 5 and a heat release factor from 2 to 5. Turbulence characteristics were obtained using Particle Image Velocimetry technique under reacting conditions, for both turbulent velocity and integral length scale and the OH-PLIF signal provided the scalar information to distinguish between burned and unburned gases. The measurements of the scalar fluxes were evaluated using different processing techniques from PIV and the effects of the grid and processing methods are first discussed. In the present investigation, both counter gradient diffusion and gradient diffusion were measured. Preheated mixtures lead to gradient diffusion due to the lower thermal expansion. Non-preheated flames exhibited counter gradient diffusion behavior except for flames with the lowest equivalence ratio. Comparisons with classical transition criterion based on Bray and modified Bray numbers were not successful for the present data set. Therefore, to correctly predict the transition between gradient and counter-gradient diffusion, a modification to the criterion taking into account pressure gradients effects was proposed. This criterion was also successfully tested with previously published results for which the integral length scales were smaller so as to encompass a wider range of turbulence scales. Furthermore, three different fuels (methane, propane and hydrogen) were used to obtain the new transition, validating the approach over a wide range of situations.

*Keywords*: Low-swirl burner, PIV, OH-PLIF, conditional measurements, BML model.

## 1. Introduction

Reducing pollutant emission from land-based gas turbines is one of the main problems industries have to face. Using lean premixed combustion systems can ease achieving the current regulations by having a lower flame temperature and therefore a lower thermal NOx emission. However, such flames are known to be unstable and a detailed description of their dynamics is an important issue for active control strategies.

Under the flamelet concept, the Bray-Moss-Libby model may be used to compute the behavior of turbulent premixed flames. One of the unclosed terms in this model is the turbulent scalar flux ($\widetilde{\mu''c''}$).

Traditional expression will relate this flux to a gradient type formulation, assuming gradient diffusion (this flux is then positive). However, recent results obtained both in numerical simulation [1] and in experimental research [2] reported two phenomena, mean velocity of burned gas higher than the one of unburned gas (known as counter-gradient diffusion or CGD in the following) and opposite behavior, namely gradient diffusion (or GD). To overcome this problem, an expression linking $\widetilde{\mu''c''}$ with the slip velocity between burned and unburned gases may be used and this allows handling both counter-gradient events and gradient events. A transition from CGD to GD is expected to happen for Bray numbers of the order of

* 平成 18 年 12 月 20 日受付（Received 20 December, 2006）

*1 Aeroengine Technology Center, Institute of Aerospace Technology

unity [1]. The classic Bray numbers involves the ratio between gaseous expansion associated to the heat release and the turbulent velocity of unburned mixture coupled to an efficiency parameter α (see equation 1).

$$Nb = \frac{\tau S_l}{2\alpha u'} \quad (1)$$

This later is function of length ratio between turbulence and flame front thickness and typical values are obtained from numerical results [1].

The scalar fluxes involved in premixed combustion are usually referred with respect to a Favre mean progress variable that is either temperature or mass weighted [2]. In recent years, some experimental investigations have been reported on Bunsen flames [2] or stagnation flames [3] or for fuel such as methane, propane and hydrogen [4]. In experiments, the easiest progress variable is a Reynolds mean (a simple time averaged description of the flame front as in [5]), but within the assumption of thin reaction zone, one may relate it to a Favre mean progress variable [3]. The typical ratio between turbulent fluctuations and laminar flame speed velocity were ranging from 1 to 6 for premixed methane-air flames and the heat release factor was kept quite high (around 6 by using only ambient temperature mixtures). Based on those experiments (all done with ambient temperature as inlet temperature), a modified criterion has been introduced and compared with available data, giving satisfactory results [3]. Its expression is given in equation 2 where the main modification lies in including length scales ratio rather than the efficiency parameter.

$$Nb^* = 0.83\tau\left(\frac{S_l}{u'}\right)^{0.75}\left(\frac{\delta_{th}}{l_f}\right)^{0.25} \quad (2)$$

However, many industrial applications have preheated air-methane as main mixture and it is interesting to see the experimental behavior of such flames as far as scalar fluxes are concerned. Having preheated mixture lowers the heat release factor and therefore encourages GD behavior. In the present case, premixed methane-air flames are investigated, with different heat release factor obtained by changing the inlet temperature. The next section introduces the burner in which experiments are done. The third part deals with the experimental techniques for conditional velocity measurements, Particle Image Velocimetry and OH-PLIF. The conditional velocities are reported for eight different flames (six under ambient temperature and two with preheated mixture). Favre fluxes are used to allow a discussion on transition between gradient and counter-gradient diffusion. Finally, a novel empirical expression for transitions is proposed that satisfactorily predicts the present results as well as previously published results.

## 2. Low swirl burner configuration

In the present case, premixed methane-air is studied under different turbulent levels as well as different heat release factor. To have a stable flame front without any external forces (like pressure gradients) or heat losses, a combustor providing stable freely propagating flames is used. It is similar to the low-swirl burner (LSB) as proposed in [6] but presents some differences, especially in the generation of turbulence. It allows planar flame stabilization under moderate and high turbulent intensity. The air may be heated up to 600K before entering the mixing chamber and a thermocouple is placed after the mixing chamber to measure the inlet temperature of the mixture (set to 590K in the present investigations).

The mass flow rate of both air and methane are set using mass flow controller (Kofloc). If preheated mixture is used, a thermocouple placed near exit of the swirl is used and its value is continuously acquired via an acquisition system PC. The results are that typical fluctuations of equivalence ratio are lower than 0.005, the uncertainties in inlet velocity are of the order of 0.01 $m.s^{-1}$ whereas temperature fluctuations are within 2K. Four secondary swirl jets are used to help stabilizing the flame by changing the mean flow divergence of the outer part of the jet. Each of the nozzle can be adjusted so that the flame stabilization plane remains as horizontal as possible. Their size is 2mm with an angle of 20 degrees with respect to the incoming flow. The inner core of the main flow remains mainly one-dimensional as velocity measurements show. The four swirl jets have a total mass flow rate between 50 and 80 $Nl.min^{-1}$, the exact value is being adjusted so that the flame front stabilizes in the measurement window for the different conditions studied. This secondary injection has no influence on the main equivalence ratio for the region studied hereafter. In the present cases, the main

mixture has a total flow rate of 667 Nl.min$^{-1}$ (881 for the flame P2). The inner diameter of the combustor is 53mm and its outer one is 60mm. To change the turbulent intensity versus laminar flame speed, different punching plates are used, differing in their blockage ratio (from 77% with holes of 1mm and a pitch of 2mm to 60% with holes of 2mm and a pitch of 3 mm and 64% for a diameter of 5mm and a pitch of 8mm as displayed in Figure 1). This is the main difference with respect to the original LSB configuration, where a slit is used to create turbulence.

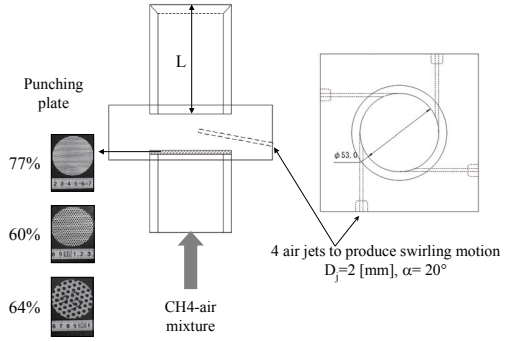


Figure 1 Schematic view of the low-swirl burner used as well as photographs of the perforated plates

A detailed sketch of the combustor can be seen in Figure 1 as well as pictures of the different punching plates used (from top to bottom plates with 1,2 and 5mm holes).

The present experimental results have all been obtained using an extension length L of 90mm. The role of this length is to modify the turbulent levels at the flame front and therefore to modify also the lifted height of the flame. A smaller length can sustain lower values of stoichiometry than longer extensions by reducing the lifted height for identical stoichiometry, however flames are less stable due to higher turbulent levels. The overall uncertainties coming from the different flow meters account for about 1% in the incoming equivalence ratio.

## 3. Experimental approach

### 3.1 Hardware

The conditional velocity measurement requires the simultaneous determination of instantaneous velocity and flame front position. Therefore a combined Particle Image Velocimetry / OH-Planar Laser Induced Fluorescence (PIV / OH-PLIF) system is well suited for this measurement. The measurement system for the PIV is composed by a mini Nd:YAG laser (from new wave research) firing at a maximum frequency of 15Hz with an energy of 120mJ per pulse. The flash lamps are actually ran at 15 Hz whereas the Q-switch command is fully synchronized with the whole acquisition system at a lower frequency. The camera used is a TSI 1K by 1K with a dynamic range of 8bits. An interferential filter centered on 532nm is used to remove the natural emission of the flame and therefore to improve signal to noise ratio. Typical field of views are 25mm$^2$, which gives a magnification of 0.025mm$^2$/pixel and the time delay was set to 60μs.

Tracer particles should be able to support high temperature, have a good reflectivity and be light enough to have a low Stokes number.

Those considerations lead to the choice of Microspehricalfeather particles MSF-30M (from Osaka Gas) with an apparent density of 0.45 and typical mean diameter of 2.7 $\mu$m. Their white color provides a high reflectivity and typical flow rate used to seed the entire combustor was limited to 3 Nl.min$^{-1}$ for all cases. The PLIF system is composed by a Spectron Laser Systems model SL 825G-400 mJ together with a dye laser Spectron Laser Systems – 4000G (Rhodamine 590) which output wavelength was set to 283.6386 nm with an energy of 20mJ after the KDP to excite OH transition. An ICCD (Princeton Instruments 576G/1) is used to capture the images of PLIF, with an UV-Nikkor 105mm/f4.5 lens. Its resolution is 576 by 384 pixels and typical measured area were 30mmx20mm, which gives a magnification 0.05 mm$^2$/pixel. It is used in gate mode with an exposure of 2 $\mu$s, synchronized with the pulse of the dye laser to minimize natural chemiluminescent emission. Lower exposure times were not possible with this ICCD, however, natural chemiluminescence of OH* was negligible compared to the signal obtained by the PLIF system. A set of band pass filters is used in front of the lens so that only fluorescent light is measured (combination of band pass Schott UG-5 and high-pass Schott WG-305 to remove Mie scattering from seeding particles). Both systems were synchronized via a BNC (Berkeley Nucleonics pulse generator, Model 555) so that the OH-PLIF laser shot was obtained exactly between the two PIV pulses and typical firing frequency was 1.2Hz to allow transfer of the data into the memory of the PC. Each time, 70

images are stored and then saved on disk before restarting the acquisition. This operation is repeated six times for the different conditions leading to typically more than 400 images for data conditional averaging purpose and measurements of turbulent velocity as well as integral length scale. A typical pair of images is shown in Figure 2.

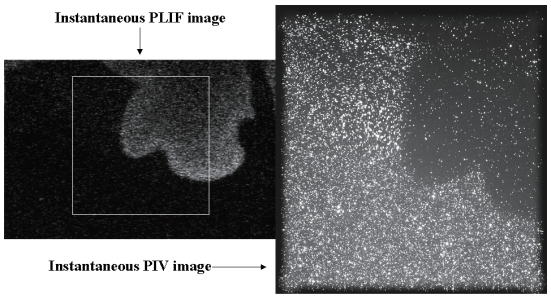


Figure 2 Instantaneous images of OH-PLIF and Mie scattering

### 3.2 Software

The images obtained with the cross-correlation camera are processed with Insight©, which incorporates an iterative box-offset feature as well as the so-called Hart correlation [7]. This allows correlation windows as small as 16x16 pixels with typical displacement of 8 pixels, as the starting correlation window is 64x64. PIV algorithms rely on the fact that all particles follow perfectly the flow and that the flow within the interrogation window remains uniform. The turbulent properties of the fresh gases reaching the flame front are obtained using PIV results for both fluctuating component and integral length scale using a two-point correlation technique on each instantaneous image. As iterative measurements as well as small correlation windows are used (with 50% overlap), the typical uncertainties of the PIV measurements remain limited to a small fraction of pixel. As the time delay between each pulse is set to be 60 $\mu$ s and as the resolution is 0.025mm$^2$/pixel, the uncertainties in the measurements remain limited to 0.05 m.s$^{-1}$. Using PIV results to obtain turbulent statistics require checking the convergence of the quantities measured. As the quantities have to be measured in fresh gases only, the available number of points is a function of the spatial position within the frame. Points close to the exit of the burner will be almost always in fresh gases whereas further downstream the probability to be in fresh gas condition is decreasing. The position for which the turbulent quantities are computed is the closest point to the exit of the burner for which the total number of samples can be used. This will be located in unburned gases with a probability to have burned gases of zero.

The principle of measurement of the integral length is the two-point correlation method.

$$f(y) = \overline{v'(y_0)v'(y_0+y)} \Big/ \overline{v'(y_0)^2}$$
$$l_{yy} = \int_0^\infty f(y)dy \qquad (3)$$

In the present conditions, only fluctuating velocities corresponding to fresh gases are used to compute the correlation and afterwards the integral.

The OH-PLIF is used to measure a time averaged mean progress variable. Each instantaneous image is divided into burned and unburned gases. The frontier between the two is taken at a value of half the maximum of the OH planar emission. Special treatment applies for burned regions far from the flame front that exhibit a lower intensity than this threshold so that they are taken into burned gases region. This is done by considering that burned gases have to be bounded by two sharp edges (one with increasing intensity and the other one with decreasing intensity). A typical example of processing choice is presented here. One may either first create a burned and unburned Mie scattering images and then perform the PIV correlation on each subsequent set of images, or perform the PIV algorithm on the raw Mie scattering images and afterwards, decide to attribute the velocity to either burned or unburned gases according to the results of PLIF. For this second version of the process, a further degree of freedom is available as one may either attribute the velocity computed inside a small window to the gases, which occupy the largest area, or to the type of gases in which the point corresponding to the center of intensity is laying. The first approach is aiming at anchoring the velocity vector not to the center of the cell but rather to the origin of the signal. This re-localization of the velocity vector is explained in Figure 3. On the left side stands the standard approach, for which the velocity is assigned to the center of the correlation window. However, it seems obvious that in

this case, the major part of the signal comes from the bottom of the correlation window, as more particles are to be found. Therefore, in case of velocity gradient (which is the case in combustion), one may obtain more reliable results when re-localizing the velocity (right side of Figure 3). Afterwards, the signal of OH-PLIF is used to assign the re-localized vector to either burned or unburned gases.

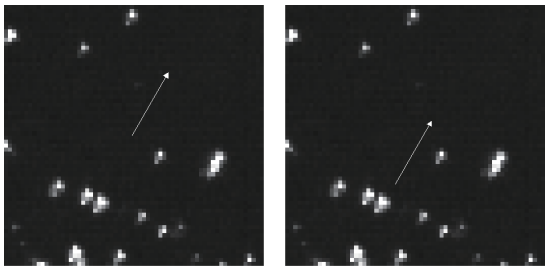

(a) Standard localization (b) Re localization result

Figure 3 Re-localization procedure of velocity field

The three different processes (two different PIV processing, using OH-PLIF on single PIV processing but on regular grid or on re-interpolated grid) are detailed on one specific example. First, for each image, three sets of PIV processing using the same conditions are used. First, the original images (two first images from the left on Figure 4) are decomposed into unburned (image 3 and 4) and burned (image 5 and 6). Afterwards, each set are processed individually.

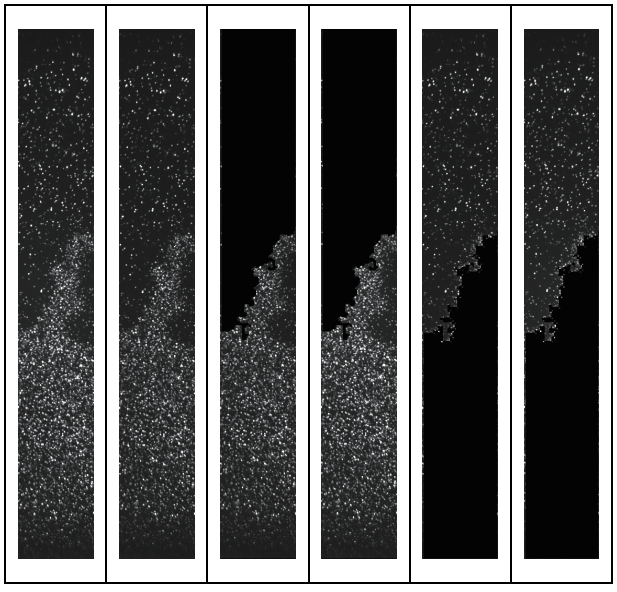

Figure 4 Three different sets of PIV processing

The approach of performing PIV processing on burned and unburned images only enables to measure almost at the same point two different velocities (as seen in Figure 5). The red vectors correspond to bunred gases, whereas green vectors are for unburned gases. One can notice that near the flame front, both burned and unburned velocities are measured.

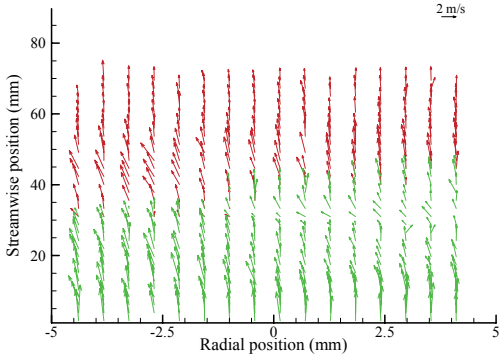


Figure 5 Conditional velocity measurements

This is not the case when processing only the overall Mie scattering images, as the output from the PIV processing results in uniformly distributed vectors (Figure 6).

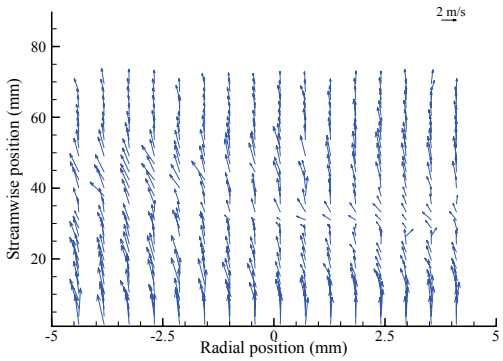


Figure 6 Non-conditional velocity measurements

It is possible to show that the main differences between the two approaches is close to the flame front, as seen in Figure 7, for which the flame front may be estimated as the region for which both burned and unburned gases are measured.

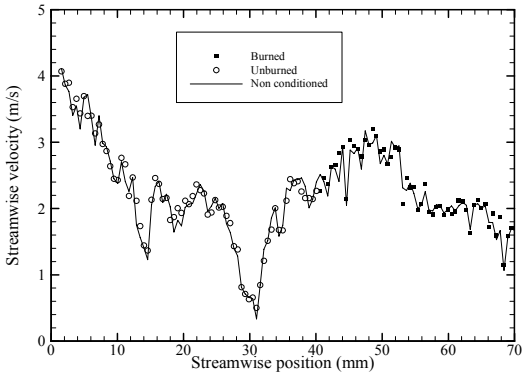


Figure 7 Comparisons on one typical profile

Finally, it is still possible to assign burned and unburned velocity from the overall Mie scattering PIV processing. The three possible approaches are compared on the mean velocity profile for flame A2. The streamwise velocity profile (see Figure 8) shows very similar values far from the flame front, but typical discrepancies appear for a streamwise position of 25mm and greater. The conditioned PIV (processing of unburned gases only) tends to provide lower velocity than the processing of the overall Mie scattering images. This may indicate over-estimation of unburned velocity, due to the presence in the correlation of particles belonging to burned gases, which is not the case for unburned PIV. No clear differences are found as far as the two discriminating method are concerned.

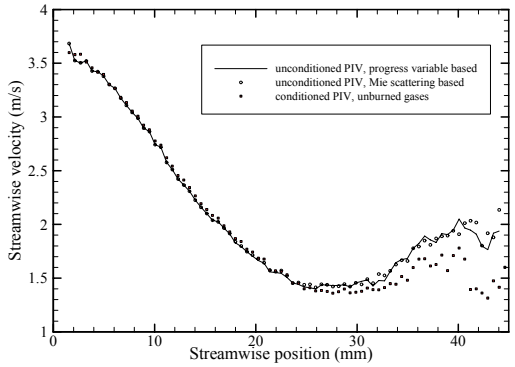


Figure 8 Mean unburned gases

Similar processing leads to the mean profile of burned gases, as displayed in Figure 9. In this case, similar results are found for streamwise position higher than 40mm, far from the flame front.

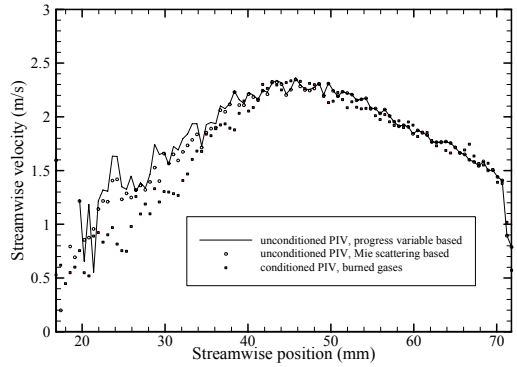


Figure 9 Mean unburned gases

Finally, when looking at the velocity difference between burned and unburned gases (Figure 10), one can see that the PIV conditioned is relatively different from the two other approaches, even though the sign of the difference is not affected by the type of processing. It must also be seen that a conditioned based on a re-localization of the velocity field enables to have results which are a bit closer to the burned-unburned PIV, as compared to a condition based on the OH-PLIF signal alone.

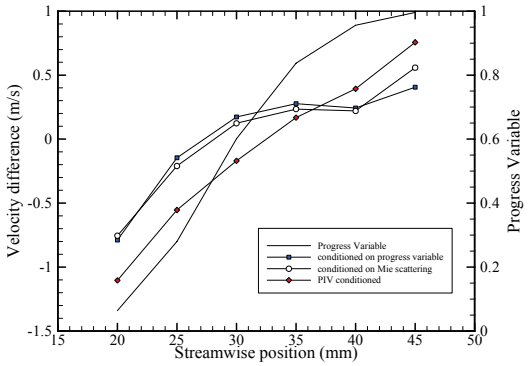


Figure 10 Velocity differences

In the following, a double sets of PIV will be used to compute the Favre fluxes for the different flames studied.

### 3.3 Experimental conditions

A series of 8 flames at ambiant inlet temperature as well as 2 flames with inlet temperature of 590K are studied. The conditions for the different flames are listed in Table 1, where A stands for ambient temperature and P for pre-heated mixtures. The eight methane-air flames at ambient temperature have a similar bulk velocity of 5m/s and the equivalence ratio is changed from 0.54 to 0.72. To change the turbulent properties, the punching plate is changed, providing two sets of blockage ratio. To change the location of the stabilization point, the swirl number is changed for similar plate and equivalence ratio conditions. The preheated flames have similar punching plate and equivalence ratio (0.50), but a different bulk velocity. Another important information provided in Table 1 is the ratio of turbulence scales to combustion scales. It is worth noting that the present flame front thickness reported here is the one required by the modified expression of the Bray number and its expression is:

$$\delta_{th} = \left(T_{ad} - T_u\right) / \left|\nabla T\right|_{\max} \qquad (4)$$

However, to classify the flame in the turbulent premixed diagram, the flame front thickness is defined by the ratio of diffusion for which heat capacity and

conductivity are computed at the inner layer temperature and the density at the unburned temperature to laminar burning velocity, as suggested in [9]. In this condition, all those flames are in the corrugated flamelet regimes. The thermal expansion $\tau$ is computed as being the difference between the adiabatic temperature and the initial temperature dividing by the inlet temperature. It is expected that for the lowest equivalence ratio studied at ambiant temperature as well as for the two preheated flames, one may have gradient-diffusion, due to a relatively low expansion factor compared to turbulence.

The 10 flames are summarized in Table 1 with four flames with an equivalence ratio of 0.54.

Table 1 Experimental conditions of the 10 flames studied

| Flame | A1 | A2 | A3 | A4 | A5 | A6 | A7 | A8 | P1 | P2 |
|---|---|---|---|---|---|---|---|---|---|---|
| $\phi$ | 0.54 | 0.54 | 0.54 | 0.54 | 0.63 | 0.63 | 0.72 | 0.72 | 0.50 | 0.50 |
| $T_e$(K) | 293 | 293 | 293 | 293 | 293 | 293 | 293 | 293 | 590 | 590 |
| Blockage ratio | 60 | 77 | 77 | 77 | 77 | 60 | 60 | 77 | 64 | 64 |
| Swirl | 1.70 | 1.14 | 1.51 | 1.47 | 1.41 | 1.61 | 1.44 | 1.32 | 1.39 | 1.35 |
| $U' / S_l$ | 4.46 | 5.25 | 5.67 | 6.53 | 4.08 | 2.83 | 2.12 | 2.64 | 1.45 | 1.85 |
| $L/\delta$ | 10.03 | 7.76 | 9.52 | 6.45 | 10.94 | 17.02 | 23.06 | 14.83 | 23.92 | 22.48 |
| $\tau$ | 4.44 | 4.44 | 4.44 | 4.44 | 4.91 | 4.91 | 5.39 | 5.39 | 1.73 | 1.73 |
| $\alpha$ | 0.85 | 0.75 | 0.82 | 0.70 | 0.88 | 1 | 1 | 1 | 1 | 1 |
| Nb | 0.59 | 0.56 | 0.48 | 0.49 | 0.68 | 0.86 | 1.27 | 1.02 | 0.60 | 0.47 |
| Nb* | 0.67 | 0.64 | 0.57 | 0.57 | 0.78 | 0.91 | 1.16 | 1.10 | 0.66 | 0.56 |
| CGD/GD | CGD/GD | CGD/GD | CGD/GD | GD | CGD | CGD | CGD | CGD | GD | GD |

## 4. Results

### 4.1 Detailed presentation of one case

Different parameters may influence the final results obtained and therefore great care has to be put on evaluating first the influence of each of the parameters. Among them, one may cite the spatial resolution used to derive the velocity, the number of samples used to compute the mean velocity as well as the turbulence properties. The study presented here is obtained for flame A3, as described in Table1.

#### 4.1.1 Number of samples

An important quantity to check is the actual convergence of both mean and turbulent velocity as function of the number of samples used. The convergence has to be checked on both the unburned, burned gases velocity and on the resultant differences between burned and unburned gases.

As far as mean convergence is concerned, the point chosen is located at X=0mm and Y=28.3mm. This point corresponds to the position for which the Reynolds-mean progress variable is 0.5. A Hart correlation with a window of 16x16 is used to illustrate the convergence. Results are presented in Figure 11 and one can notice that a convergence is readily obtained for unburned gases samples after about 200 samples, whereas convergence is more difficult to obtain for burned gases. The reason is that

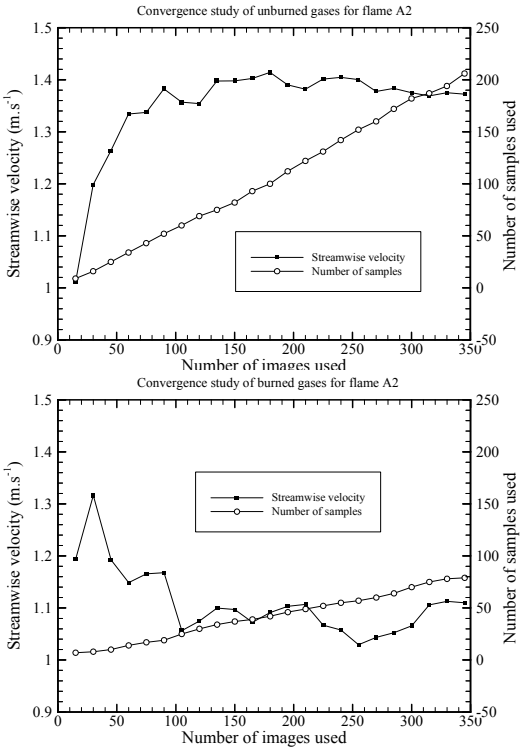


Figure 11 Convergence study for mean velocity of unburned and burned gases

whereas 350 images are used, only 80 images lead to a validated measurement of velocity for the burned gases.

This may have strong influence on the final results, as too few samples may lead to a wrong conclusion as far as scalar flux is concerned. This is illustrated in Figure 12 where the difference in streamwise velocity is plotted for the flame A2 as function of the number of images actually used to compute the difference between product and reactant velocity. One can see that for few samples used, counter-gradient type diffusion is measured (as burned gases have a higher velocity than unburned), whereas the situation is inverted and reaches a constant value for 300 or more samples. A decent approximation may already be obtained for 100 samples, which was typically the number of images used by [3].

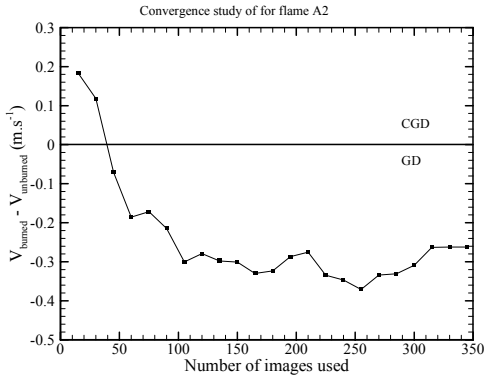


Figure 12 Convergence of velocity difference for flame A3

Another important parameter is the actual location of the point taken to compute the turbulent characteristics of the flame. In the present case, it has been decided to measure the integral length scale at the point for which the probability to have the flame front is 0.05 (or a Reynolds-mean progress variable of 0.05). The turbulent characteristics are those of the incoming fresh mixture and therefore have to be obtained in unburned gases only. The results are presented in Figure 13 for the point X=0mm and Y=20.2mm. The convergence is obtained for values around 250 samples, even though good estimated may already be obtained with as few as 100 images.

From this preliminary consideration, one can conclude that acquiring 360 samples are enough to measure accurately both mean, fluctuating components of the velocity as well as scalar fluxes.

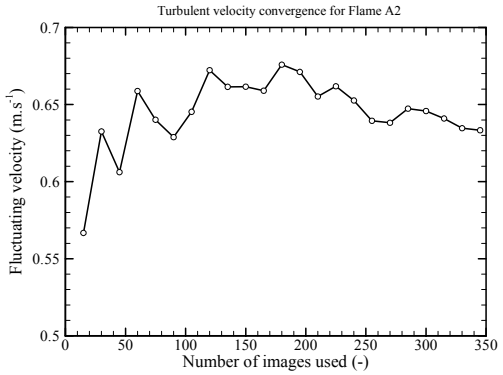


Figure 13 Convergence of turbulent velocity for flame A3

### 4.1.2 Spatial resolution

Another important aspect is the spatial resolution used. Using different PIV grid sizes allows studying the convergence of this quantity as well as the fluctuations of velocity. Both are very important to precisely define the turbulent flame. A similar approach has already been proposed ([8]). A typical concern when increasing the window size is the decrease in the signal to noise ratio that may be associated with a smaller window (hence fewer particles present in the correlation window). Such a study has been performed for one typical case, with windows starting at 64pixels (4.5mm) to 8 pixels (0.6mm). The signal between the peak of correlation and the base level signal of correlation is used to compare the influence of the grid size. Measurements obtained with a fast Fourier transform algorithm are presented in Figure 14. One can see that an increase in the window size results in a decrease of the signal to noise. This may be due to the fact that within bigger windows, the velocity gradients have stronger effects than for smaller windows. Even though the number of particles used to compute the correlation signal drops with an increase in spatial resolution, the actual signal to noise ratio increases. For the test case presented here, the flame front would be typically around Y=20mm and that explains the drop in the signal to noise ratio. This is due to the fact that the flame being a low-density region has fewer particles than reactant gases. A similar study is presented when using the Hart correlation algorithm and the results are compared with the fast fourrier transform algorithm in Figure 15. When compared with a classic approach, one can see a little increase in the signal to noise, as shown by the comparison when both resolutions are

2.3mm. An important information is that the signal to noise ratio does not suffer from a reduction in the window size (hence increased spatial resolution) even though the overall number of particles used to compute the correlation decreases. Therefore, as far as signal to noise ratio is concerned, one may go to the highest spatial resolution possible in this case, without losing accuracy.

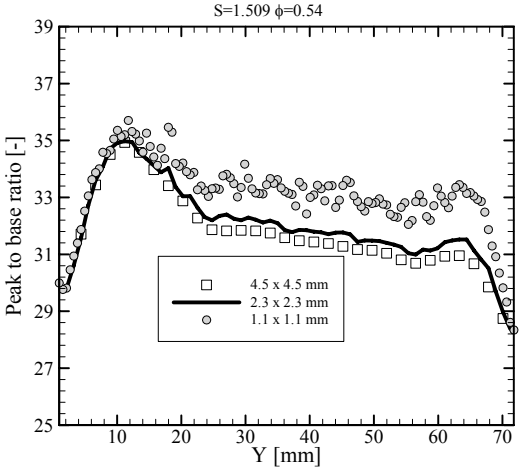


Figure 14 Effect of increasing PIV resolution on signal to noise ratio

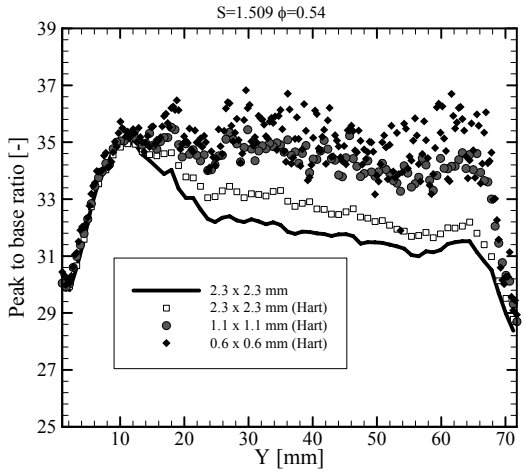


Figure 15 Effect of increasing PIV resolution with Hart correlation on signal to noise ratio

To further illustrate the influence of the spatial resolution, the mean velocity obtained at c=0.05 for unburned gases is computed as function of the spatial resolution and algorithm used. Results are plotted in Figure 16 for both fast Fourier transform and Hart correlation. One can notice that results obtained with the smallest grid are a bit higher than the other grids and therefore they should not be used. Almost no change in the mean velocity is observed between a 32x32 and 16x16 when using a Hart correlation and therefore for increased spatial resolution, one would rather use the 16x16 results. When looking at the convergence of the scalar fluxes (or at least in the present case at the difference between burned and unburned gases), one can notice on the bottom part of Figure 16 that even though the sign is well obtained independently on the grid and algorithm, no converged values are obtained. It is expected however that Hart correlation performed better in burned gasses, which is the limiting parameter when computing scalar fluxes.

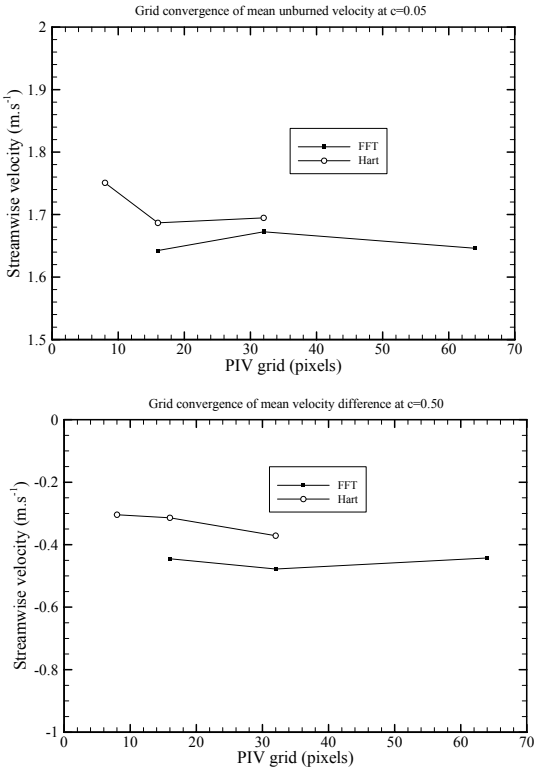


Figure 16 Grid influence on mean velocity and velocity difference

Identical conclusions may be drawn form turbulent velocity measurements with different spatial resolution. An important point is that the ratio between the integral length scale and the size of the window is large enough to have accurate estimates of both fluctuation and integral length measurements. From this analysis, it turns out that a Hart correlation based on window sizes of 16x16 will be used to compute scalar fluxes on the basis of 350 images for all conditions.

### 4.1.3 Favre-mean representation

When dealing with scalar fluxes, one has to use a Favre-mean representation of the progress variable. To obtain a Favre progress variable ($\tilde{c}$), one uses the following equation

$$\overline{c} = \rho c / \overline{\rho}$$

$$\tilde{c} = \frac{\overline{c}}{1+\tau(1-\overline{c})}$$

$$\overline{\rho} = (1-\overline{c})\rho_u + \overline{c}\,\rho_b$$

where $\overline{c}$ is the Reynolds mean progress variable and $\rho_r$ and $\rho_p$ the density of reactant and product respectively. The difference between a Reynolds mean progress variable approach and a Favre mean progress variable is illustrated in Figure 17.

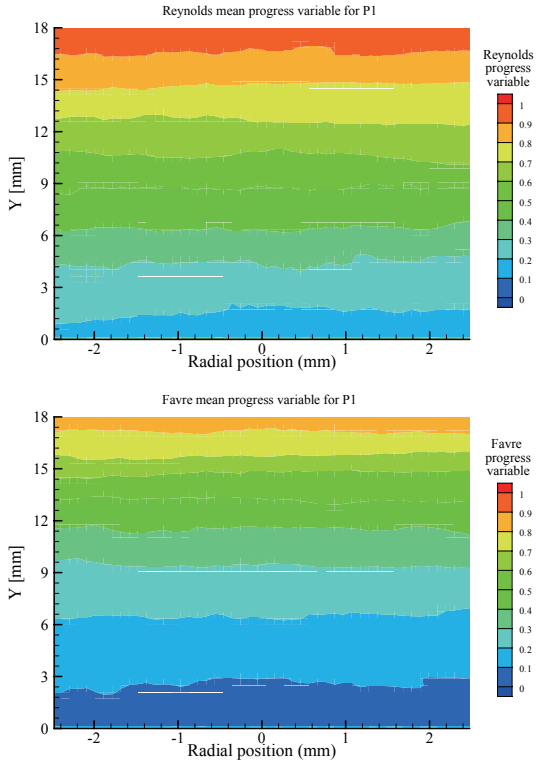


Figure 17 Difference between Reynolds and Favre mean progress variable

A one-dimensional profile is taken in the center of the burner for both progress variable and results are presented in Figure18. One can see that within the same physical space, a Favre-mean progress variable is lower than the Reynolds-mean progress variable. This will have consequences when presenting scalar fluxes as function of Favre-mean progress variable as a Favre-mean progress variable of unity may not be reached within the field of view.

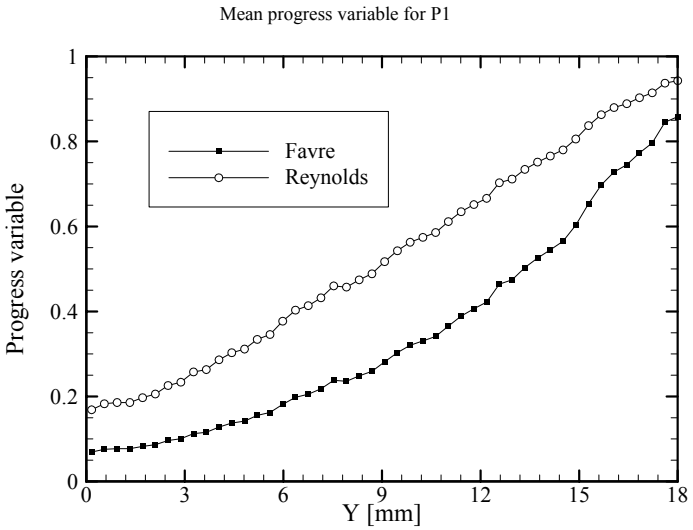


Figure 18 1D profile of Reynolds-mean and Favre-mean progress variable

## 4.2 Results for all the flames

### 4.2.1 Reynolds-mean progress variable and mean velocity field

The average over 420 shots shows the mean flame shape and position (see Figure 19) for the high heat release factor case (A1 to A8) and for preheated flames (P1-P2) on Figure 20. One can notice that the flame brush is relatively horizontal and perpendicular to the incoming mixture for radial position smaller than 2.5mm, as shown by the simultaneous velocity field. This velocity corresponds to the mean velocity of unburned gas for the different positions and the contour to the Reynolds mean progress variable for which a value of unity corresponds to a position where burned gases are always detected. From those plots, it seems possible to derive statistics on velocity along the centerline of the flow and those measurements will represent velocity perpendicular to the flame front that is the assumption for the BML model. The present analysis is restricted on radial position lower than 5mm as secondary swirling jets do influence the local equivalence ratio by inducing dilution effects. Those effects become more important with an increase of the swirl number ([11]) but remain absent in the center of the flow.

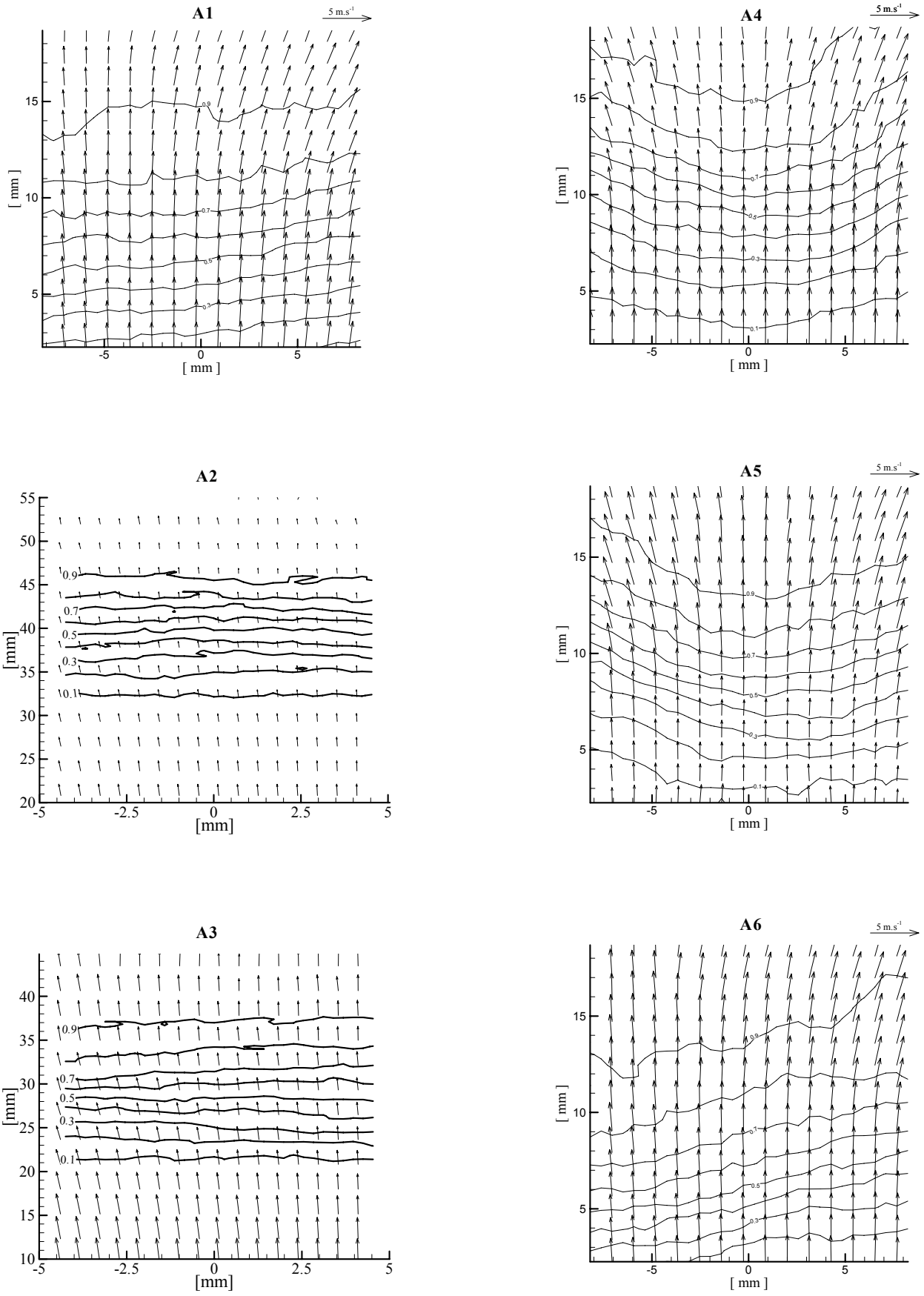


Figure 19 Mean velocity fields of unburned gases as well as Reynolds mean progress variable contours for flames A1 to A6.

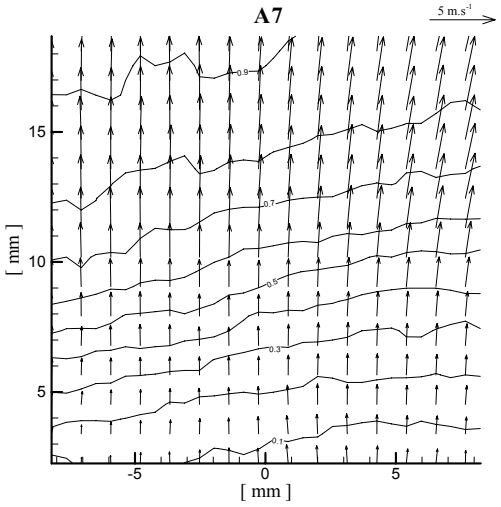


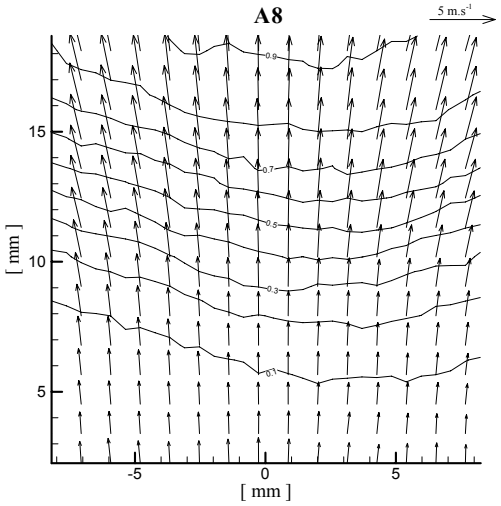


Figure 19 Mean velocity fields of unburned gases as well as Reynolds mean progress variable contours for flames A7 to A8.

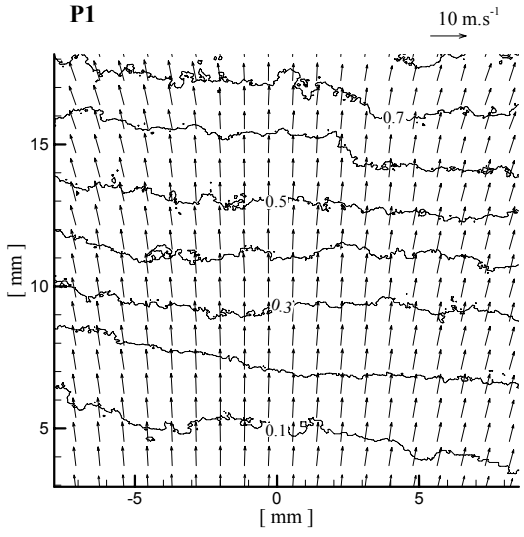


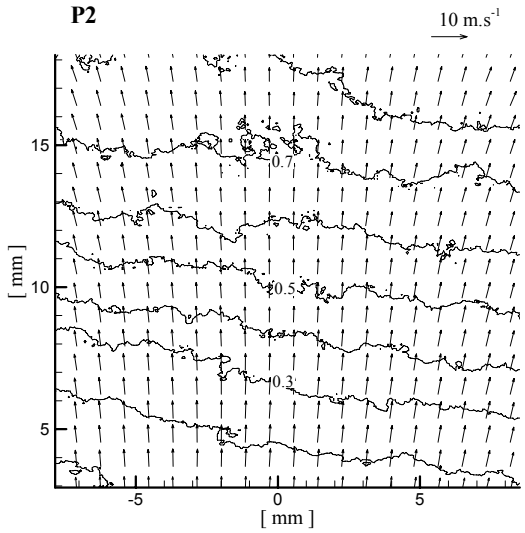


Figure 20 Mean velocity fields of unburned gases as well as Reynolds mean progress variable contours for flames P1and P2.

### 4.2.2 Velocity profile in Cartesian coordinates

The first data are presented in a Cartesian coordinates. The origin of the stream wise position is the exit of the burner. Only four flames are presented, as being representative of the different process involved. The first two flames (A2 and A3) shown in Figure 21, do present two distinctive regions. The first one, close to the nozzle for which unburned gases are faster than burned gases and the second one, further downstream where the situation is inverted.

Looking at the profiles for flame A8 one can notice that burned gases are always faster than unburned gases. Finally flame P2 exhibits an opposite behavior.

### 4.2.3 Scalar fluxes

Furthermore, it is important to notice that the integral length scales measured are ranging from 9 to 16mm. As PIV windows of 16x16 (0.6mmx0.6mm) are used to obtain those measurements, the typical ratio between the window sizes and measured integral length scales is between 0.05 and 0.025, which is small enough to have a good accuracy in those measurements. The measured fluctuating velocities are therefore also close to the true fluctuations as filtering effects by PIV becomes less important for small ratio between window size and integral length scale, as discussed in [10].

Assuming a thin reaction zone, it is possible to relate Reynolds mean progress variable and Favre

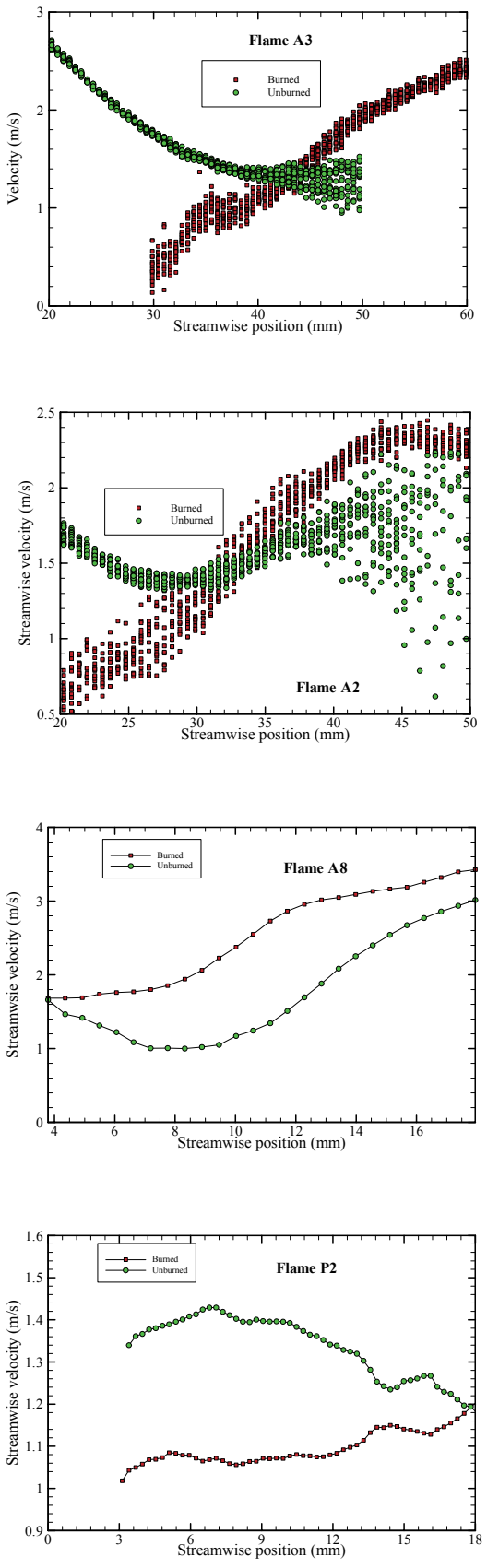


Figure 21 : Mean velocity of unburned and burned gases.

mean progress variable as shown for instance in [3]. The Favre flux can also be measured, using the Favre mean progress variable $\tilde{c}$ as well as the density of gas and the differences between the velocities of products and reactants, as shown in equation (5).

$$\overline{\rho}\widetilde{\mu''c''} = \overline{\rho}\tilde{c}(1-\tilde{c})(\overline{u_b} - \overline{u_u}) \qquad (5)$$

The results of axial Favre fluxes for the four flames with an equivalence ratio of 0.54 are displayed in Figure 22, whereas the flames for higher heat release factor are displayed in Figure 23. All points with radial distance less than 2.5 mm from the center are plotted for the different flames. One can notice that flame A4 does exhibit GD behavior whereas Flame A1, A2 and A3 shows both GD and CGD and will therefore not be considered furthermore for the discussion. It is interesting to see that flames A1, A2 and A3 have different behavior. Flame A 2 and A3, which are almost similar, have a turbulence level comprised between flame A1 and A4. The turbulence fluctuations of flame A4 are strong enough to lead to an overall gradient diffusion behavior. The turbulence levels of flames A2 and A3 are not strong enough to yield an overall gradient diffusion behavior, even though for relatively small Favre progress variable, the turbulent scalar fluxes are negative, indicating a gradient behavior. However, flame thermal expansion is not overtaken and the turbulent scalar fluxes is positive at very high Favre progress variable. Results for higher heat release (A5-A6 and A7-A8) clearly exhibit CGD behavior, heat release being the leading mechanisms. On the opposite side, using preheating mixture even under low turbulent levels, GD is clearly measured for flames P1 and P2 as shown in Figure 24.

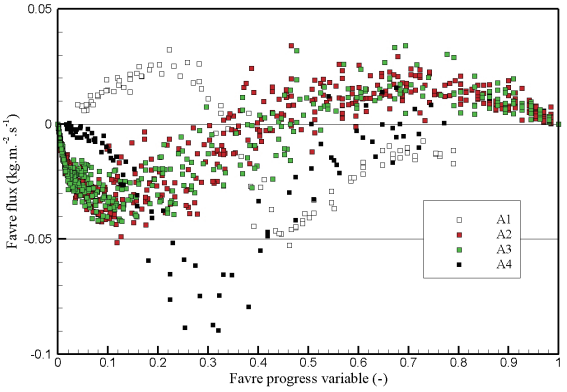


Figure 22 Favre flux measurements (axial component only) for flames A1 to A4 as function of a Favre averaged progress variable

This illustrates the heat release factor's influence on the gradient diffusion process and tends mainly to lead to GD behavior for lean premixed preheated flames, as even low turbulent intensity results in GD behavior. This type of conclusion was also derived when using 2D DNS with a heat release factor of 2.06 ([12]) and is therefore in good agreement with numerical simulations.

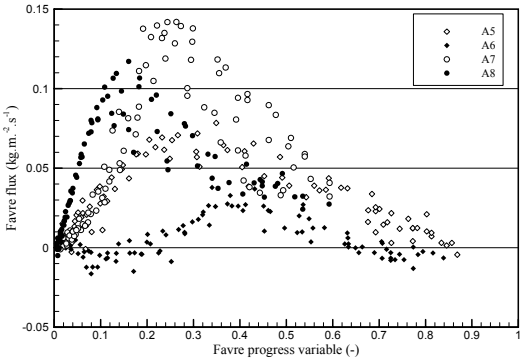


Figure 23 Favre flux measurements (axial component only) for flames A5 to A6 as function of a Favre averaged progress variable

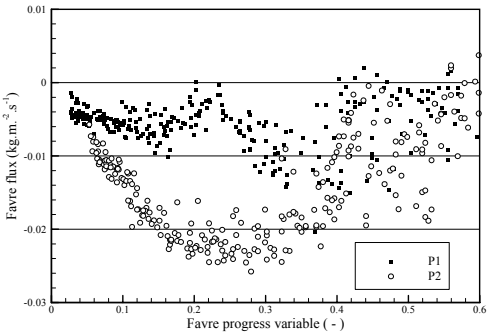


Figure 24 Favre flux measurements (axial component only) for flames P1 and P2 as function of a Favre averaged progress variable

## 5. Discussion

Using the turbulent information obtained by PIV and the flame characteristics using Premix from Chemkin with GriMech 3.0, one may compute the values of Bray numbers based on the new formulation for the efficiency parameter [5] in absence of external pressure gradients (see equation 2). Typical results are reported in Table 1, where one can notice that the new expression predicts well the behavior for P1 and P2 but lacks in predicting correctly the dynamics of the flames A2 and A5. Data for flame A4 are not computed as experimentally both GD and CGD were measured. External pressure gradients and buoyancy effects have to be taken into account and can be expressed as ([13])

$$Nb_{(p)} = Nb\left[1-\beta\frac{l_I^2}{12KS_l\nu_u}\left(-\frac{\partial\overline{P}}{\partial x}+\frac{\Gamma}{\tau+1}\right)\right] \quad (6)$$

,where K=0.8 and $\beta$ =0.12 and Nb a bray number that does not take into account the pressure effects. $\Gamma$ is the acceleration associated to gravity. Strong external pressure gradients will tend to reduce the effects associated to the thermal expansion, hence promote gradient diffusion. The term including the pressure gradients may be computed using Bernoulli's equation over fluid streamlines. In the present case, they are considered as null as the flow field changes completely from non-reacting to reacting cases and measurements in non-reacting cases would not provide a proper estimation. Furthermore, in opposite with stagnation plate experiments, no solid boundary exists and it may be fair to consider those flames as free of external pressure gradients. Therefore, in the present analysis, only gravity is considered and taken negative as g is directed toward unburned gases. Its effects will be to promote CGD, gravity being more important for unburned gases than for burned gases. Applying this modification (denoted as $Nb^*(\Gamma)$) to the present data sets did not allow a fully agreement with the experimental results, as seen in Table 1 where discrepancies still exist especially for flame A1 which has a modified bray number higher than unity. One of the possible reasons for the differences is that the proposed expression was obtained with relatively small integral length scales and therefore the exponent of the ratio between the thermal flame thickness and the integral length scale did not have an important weight. The present data are obtained for much larger ratios and therefore a way to improve the prediction is to slightly modify the different exponents. Using the present data sets and results reported in [6], a new criterion is proposed:

$$Nb_z(p,\Gamma) = 0.88\tau\left(\frac{S_l}{u'}\right)^{0.80}\left(\frac{\delta_{th}}{l_f}\right)^{0.28} f(p,\Gamma) \quad (7)$$

Predictions for the current data sets are reported in

Table 1, where one can indeed notice the improvements compared to expression shown in equation (2). The new Bray number changed from 1.07 to 0.99 for flame A1. Equation 7 gives satisfactory results for the present data set. In Table 1, the new expression's values without taking into account the external pressure gradients are also reported. To verify that this new expression is also valid for other cases, the transition for the flames reported in [3] were also predicted. The referred results were obtained for methane and propane and typical integral length scales ranging between 1 and 2mm and with ratios of turbulent velocity to laminar flame speed between 1.2 and 5.4. The setup consisted in a stagnation plate experiments for different flow rates (mean velocity of 2.7 and 5.0 m/s). Data from Bunsen flames (initially reported in [2]) are used together with the integral length scale ratios reported in [14] for two of the flames (namely B and D in [2]). Data taken inside premixed Bunsen flames with lean hydrogen/air mixtures ([4]) are also considered for the new expression. Those data have similar ranges of ratios as the present study (length scales over 10, velocities ratios over 4.5). The overall results, covering the three referred papers and the present data are presented in Figure 25.

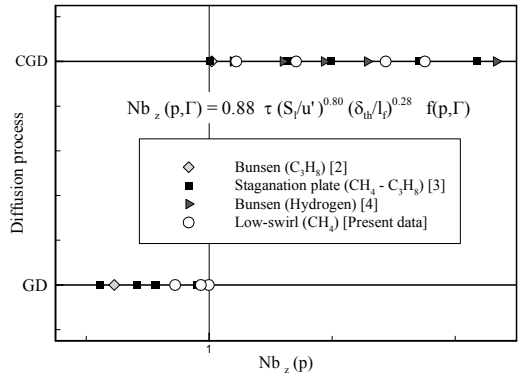


Figure 25 Summary of transition criteria based on present and previous data sets

The horizontal axis represents the new modified bray number computed based upon the different measurements. The circles correspond to the present data set and the other symbols represent the different experimental results obtained previously ([2]-[4]). The vertical axis represents the actual diffusion process measured. One can notice that all data sets have a transition between GD towards CGD for values of $Nb_z(p,\Gamma)$ close to unity. The proposed transition works not only for the present data set (large integral length scales) but also for cases having smaller length scales ([3]). It is able to correctly predict the diffusion process in Bunsen type flames, stagnation type and low-swirl burner type, covering a wide range of flow configurations and three different fuel: methane, propane and hydrogen for different heat release factor.

## 6. Conclusions

Joint PIV/OH-PLIF techniques could successfully be performed in premixed (non-preheated and preheated) methane-air mixture for flames sustained by a low-swirl burner. The simultaneous measurements of planar velocity and planar OH were used to measure conditional velocities for eight different flame configurations. OH was used to distinguish between burned and unburned gases whereas PIV was used not only to compute conditional velocity but also to compute the characteristics of turbulence in unburned gases. Based on those planar imaging techniques, both gradients and counter-gradients measurements were obtained. Assuming thin reaction zone as required for BML model, Favre flux derivations showed that using preheated mixture encouraged gradient diffusion process through a lowering of the heat release factor even when keeping a low level of turbulence (ratio from 1 to 6). Non-preheated flames on the other hand were mainly having CGD except those for the lowest equivalence ratio who showed GD behavior, again a lower heat release being responsible for the shift between CGD towards GD when using leaner mixtures. Predictions based on measurements of ratios between flame and turbulence length scale and velocity were tested on the present data sets. It turned out that to better predict the diffusion process, gravity effects had to be taken into account. However, as discrepancies were observed between previously available transition criteria, a novel transition parameter was developed. The newly introduced number was successfully tested in the present data sets as well as previously published results. As it has also been evaluated for other conditions, one may conclude that the introduced transition criterion is able to cover

a wide range of integral length scales and heat release factors, still remaining in the thin-flame assumption, as required by the BML model. The fact that similar transition applied for three different fuels suggests that Lewis number does not play a role for the transition from GD to CGD.

## 7. References

[1] D. Veynante, A. Trouve, K.N.C. Bray, T. Mantel, *J. Fluid Mech* (1997) 332:263-293.

[2] P.A.M. Kalt, Y.-C. Chen, R.W. Bilger, *Proc. Combust. Inst*. 27 (1998) 751-758.

[3] P.A.M. Kalt, Y.-C. Chen, R.W. Bilger, *Combust. Flame* (2002) 129:401-415.

[4] Y.-C. Chen, R.W. Bilger, *Proc. Combust. Inst*. 28 (2000) 521-528.

[5] J.H. Frank, P.A.M. Kalt, R.W. Bilger, *Combust. Flame* (1999) 116:220-232.

[6] B. Bedat, R.K. Cheng, *Combust. Flame* (1995) 100:485-494.

[7] D.P. Hart, *Exp. Fluids* (2000) 29:13-22

[8] S. Jeon, S. Tachibana, L. Zimmer, A. Nishizawa, *Development of an active grid adapted to the low-swirl burner and measurements of turbulent properties of the flow field*, JAXA-RR-05-055E (March 2006)

[9] N. Peters, *Turbulent combustion*, Cambridge University Press, New York, 2000.

[10] A. Hoest-Madsen, A.H. Nielsen, *Accuracy of PIV Measurements in Turbulent Flows*, ASME Laser Anemometry, FED-Vol. 229, 1995.

[11] L. Zimmer, S. Tachibana, *Laser Induced Plasma Spectroscopy for Local Composition Measurements Inside a Low Swirl Burner*, *20th International. Colloquium on the Dynamics of Explosions and Reactive Systems. Montreal, 2005*.

[12] N. Swaminathan, R.W. Bilger, B. Cuenot, *Combust. Flame* 126 (2001) 1764-1779.

[13] D. Veynante, T. Poinsot, *J. Fluid Mech* (1997) 353 (1997) 83-114.

[14] Y.-C. Chen, P.A.M. Kalt, R.W. Bilger, N. Swaminathan, *Proc. Combust. Inst*. 29 (2002) 1863-1871.

**JAXA Research and Development Report JAXA-RR-06-020E**

Date of Issue : March 30, 2007
Edited and Published by : Japan Aerospace Exploration Agency
7-44-1 Jindaiji-higashimachi, Chofu-shi, Tokyo 182-8522 Japan
URL: http://www.jaxa.jp/
Printed by : BCC Co., Ltd.